ROYAL SOCIETY
OF CHEMISTRY

PAPER

Check for updates

Mutagenesis-based evolution enables rapid retargeting of L-aptamers for structured RNA recognition

Xuan Han, [ID][a] Tyler Guilbault[a] and Jonathan T. Sczepanski [ID] *[ab]

Mirror-image L-(deoxy)ribose nucleic acid aptamers (L-aptamers) enable high-affinity, selective recognition of native structured RNAs *via* shape-based, cross-chiral interactions rather than Watson–Crick base pairing. However, achieving this level of specificity has typically required *de novo* selection from fully randomized libraries for each new target. Here, we report the first application of mutagenesis-based evolution to an existing cross-chiral L-aptamer to rapidly reprogram target specificity. Starting from a parental aptamer recognizing the HIV-1 TAR RNA hairpin, we generated two evolved aptamers that, together with the parent, form a set of orthogonal binders capable of discriminating RNA hairpins differing by a single nucleotide. Deep sequencing revealed that retargeting requires extensive remodeling of the aptamer fold rather than incremental sequence changes, reflecting the dependence of cross-chiral interactions on global RNA architecture rather than local sequence complementarity. Finally, RNA pulldown experiments demonstrate that these orthogonal L-aptamers retain strict selectivity in a competitive and structurally complex context, including extended flanking sequences and multiple RNA targets. Taken together, this work establishes mutagenesis-based evolution as a versatile strategy for rapidly retargeting cross-chiral L-aptamers and reinforces the unique advantages of structure-based RNA recognition, providing a framework for developing adaptable and multiplexable RNA-targeting strategies.

Introduction

Due to its single-stranded nature, RNA can form complex three-dimensional structures driven by intramolecular base pairing interactions.[1] These structures, which include helices, loops, and bulges, facilitate interactions with proteins and other RNAs, enabling participation in critical regulatory and gene expression processes. Recent research has increasingly demonstrated relationships between structured RNAs and diverse disease states, including cancer,[2–4] viral infection,[5–7] neurological disorders,[8–10] and immune responses.[11,12] These discoveries have made structured RNAs attractive targets for both diagnostic and therapeutic applications.[13–15]

Traditionally, RNA is targeted using hybridization-based technologies, such as antisense oligonucleotides (ASOs) or small interfering RNAs (siRNAs); however, the inaccessibility of sequences within pre-existing structures presents significant challenges to these methods.[16] Structural-based approaches

and helper strands can be implemented to increase potency, but these strategies still do not fully overcome barriers posed by more stable RNA structures. Small molecules have emerged as a promising platform for targeting RNA structures. In recent years, small molecules targeting distinct structural elements with specific sequences have progressed from laboratory research to FDA-approved drugs.[17] Nevertheless, the discovery of RNA-binding small molecules with high affinity and structural specificity remains challenging due to RNA's negatively charged backbone, inherent flexibility, and structural redundancy. Limited structural data for nucleic acid further limits the structure-based approach using small molecules.[15]

A promising alternative is the use of aptamers—nucleic acid sequences selected to bind target ligands with high specificity and affinity. The process used to generate aptamers, systematic evolution of ligands by exponential enrichment (SELEX),[18] allows for the discovery of aptamers against targets ranging from single metal ions[19] to whole cells.[20,21] Notably, work from our group and others[22–29] has shown that aptamers composed of L-DNA or L-RNA, which are the synthetic enantiomers of natural D-nucleotides, can be evolved to bind tightly to RNA structures, and may be particularly well suited for this purpose. Although D- and L-oligonucleotides share identical physical and

[a] *Department of Chemistry, Texas A&M University, College Station, Texas, 77843, USA. E-mail: jon.sczepanski@chem.tamu.edu*

[b] *Department of Biochemistry and Biophysics, Texas A&M University, College Station, Texas, 77843, USA*

chemical properties, they cannot form contiguous Watson–Crick base pairs with one another. As a result, so-called "cross-chiral" interactions between D- and L-oligonucleotides must occur independently of primary sequence. This unique feature is leveraged during *in vitro* selection to evolve L-aptamers that adaptively bind structured D-RNA targets through tertiary, shape-driven interactions rather than sequence complementarity.[30] We have demonstrated that cross-chiral recognition occurs with low-nanomolar affinity and high selectivity.[22–26,31] Notably, L-aptamers can distinguish their cognate D-RNA targets from those with single-nucleotide substitutions or small structural perturbations.[22,24,30] Combined with the inherent nuclease resistance of L-oligonucleotides,[32] these properties position L-aptamers as versatile and powerful reagents for targeting structured RNA.

Mutagenesis-based aptamer selection is a strategy used to evolve the target specificity of an existing aptamer by deliberately introducing mutations into its sequence and then rescreening the resulting library. This differs from the standard SELEX process, which starts with a fully random library. The mutagenesis-based approach allows for fine-tuning of an aptamer's binding properties to discriminate between closely related targets or to evolve new specificity entirely.[33,34] For example, Huang *et al.* used this approach to alter an ATP aptamer to bind GTP, with aptamers binding GTP emerging after five rounds of selection from a mutagenized library against a GTP analogue.[33] Given the high selectivity of cross-chiral interactions between L-aptamers and RNA, along with their unique structure-based mode of recognition, we were curious whether mutagenesis-based selection could be used to evolve L-aptamers with altered substrate specificity. Although mutagenesis-based selection has not previously been attempted with cross-chiral aptamers, such a strategy could greatly expand the toolkit of mirror-image technologies. Not only would this provide a convenient and rapid strategy for generating L-aptamers against new RNA targets, but the results may also reveal important insights into the relationship between specificity and structure, aiding in the design of future cross-chiral L-aptamers.

In this study, we introduce mutagenesis-based SELEX as a rapid strategy for retargeting cross-chiral L-aptamers to new structured RNA targets. We show that closely related RNA structures previously disfavored by the parental aptamer can be selectively recognized without restarting selection from fully randomized libraries. Deep sequencing reveals that altered target specificity arises from extensive remodeling of the aptamer fold rather than incremental sequence adjustments, highlighting the structure-driven nature of cross-chiral recognition. Enrichment analysis further demonstrates the rapid emergence of orthogonal, highly specific L-aptamer–RNA pairs, providing a foundation for scalable and multiplexed RNA-targeting strategies.

Results and discussion

Library and target design

The aptamer chosen for this study was L-6-4t (Fig. 1a), which binds tightly (K_d = 100 ± 30 nM) to the *trans*-activation response
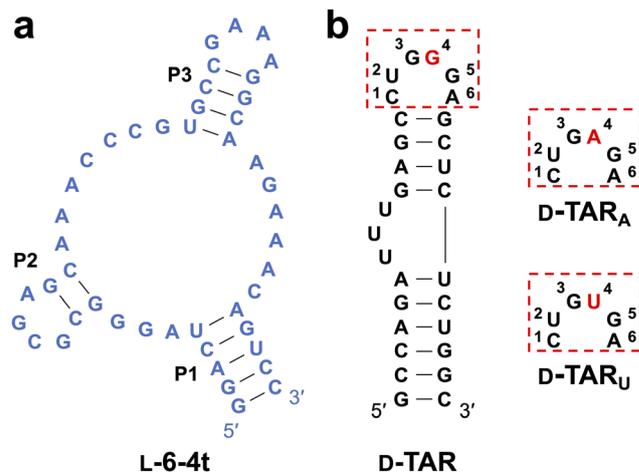

Fig. 1 Sequences and predicted secondary structures of the parent L-6-4t aptamer and its TAR RNA ligand. Black and blue lettering indicate D- and L-oligonucleotides, respectively. (a) Cross-chiral L-aptamer L-6-4t. (b) Wild-type TAR RNA and single-nucleotide variants TAR$_A$ and TAR$_U$. The boxed region denotes the distal loop domain.

element RNA (D-TAR) from Human Immunodeficiency Virus type 1 (HIV-1), shown in Fig. 1b.[23] Previous in-line hydrolysis probing showed that L-6-4t binds D-TAR through its 6-nucleotide (nt) distal loop.[23] Importantly, using a library of TAR hairpins containing all possible 6-nucleotide loops, we previously showed that L-6-4t binds with high selectively to the 5′-(C/U)UGGG(A/G)-3′ loop motif (Fig. 1b).[25] This strict sequence requirement provided an ideal opportunity to test whether we could evolve altered target specificity. Therefore, we chose to incorporate either a transition mutation (D-TAR$_A$) or transversion mutation (D-TAR$_U$) at position G4 within the invariable 6-nt loop domain (Fig. 1b). Because the distal loop constitutes the primary aptamer recognition interface, mutations within the stem region were not expected to directly impact binding specificity and were therefore not examined in this study.[23,31] We hypothesized that the overall structural change for a transition mutation would be less significant than for a transversion and, thus, would require fewer compensatory mutations within the aptamer to accommodate. We prepared L-RNA versions of these hairpins (L-TAR$_A$ and L-TAR$_U$) in which the target loop sequences were grafted onto a minimum stem scaffold to reinforce loop-based interaction (Fig. S1a and S2). As expected, an electrophoretic mobility shift assay (EMSA) revealed that D-6-4t was unable to bind the mutated L-TAR targets (Fig. S1c).

We next prepared a library of D-6-4t aptamers (D-Lib14) such that the original random sequence domain was mutagenized to a degeneracy of 14% at each position (Fig. S1b), yielding a population carrying an average of 6 mutation per member (see Methods and Fig. S3a and b). The binomial distribution strongly favors low mutation counts; consequently, unique sequences with fewer mutations are more abundant in the pool. We expected that favoring a lower number of mutations would drive repurposing of the existing structural motif rather than major structural reorganization. To facilitate the SELEX

process, the primer binding site sequences used for isolating the parent 6-4t aptamer were appended to the ends of the mutagenized library (Fig. S1b). As with the parent aptamer, D-Lib14 did not bind to either of the mutated L-TAR hairpins (Fig. S1c).

## Mutagenesis-based SELEX alters the substrate specificity of cross-chiral interaction

Similar to the isolation of the parent aptamer L-6-4t, we carried out cross-chiral mutagenesis-based SELEX using the "selection reflection" technique.[35–37] In this process, a D-nucleic acid library (i.e., D-Lib14) is selected against the enantiomer of the target ligand (i.e., L-TAR$_A$ or L-TAR$_U$), which facilitates enzymatic amplification of the library after the selection step. Once the SELEX process is complete and lead D-aptamers are identified, they can be chemically synthesized in the L-form and used to bind the intended D-RNA ligand.[35,37] Accordingly, D-Lib14 was incubated with 3′-biotinylated L-TAR$_A$ or L-TAR$_U$ (L-TAR$_A$-BIO and L-TAR$_U$-BIO, respectively; Fig. S1a and Table S1) at room temperature in the presence of 50 mM NaCl, 10 mM MgCl$_2$, 0.1% (v/v) Tween-20, and Tris (pH = 7.6). Sequences bound to a biotinylated hairpin target were immobilized on magnetic streptavidin beads. The beads were then washed thoroughly with the same buffer and bound sequences were eluted by denaturation with NaOH. Eluted sequences were reverse transcribed and amplified by PCR. The resulting dsDNA libraries were subjected to in vitro transcription to generate the corresponding ssRNA library to be used in the next round of SELEX.

During the first four rounds, selection of D-Lib14 was performed against L-TAR$_A$ and L-TAR$_U$ simultaneously to enhance SELEX efficiency. After round 4, an EMSA revealed that the enriched library had substantial affinity for L-TAR$_A$, with no detectable binding to L-TAR$_U$ (Fig. S4a). To avoid further skewing the library away from the L-TAR$_U$ target, all subsequent rounds were carried out using individual targets (referred to as "deconvolution" rounds) (Fig. 2a). Because the library was already highly enriched for L-TAR$_A$-binding sequences after round 4, only one round (round 5$_A$) of deconvolution was performed to further enrich sequences that bound to L-TAR$_A$. However, L-TAR$_U$ required four additional deconvolution rounds (rounds 5$_U$ through 8$_U$, 8 in total) before appreciable binding was observed by EMSA (Fig. S4b). Nevertheless, these results indicated that we had successfully obtained cross-chiral aptamers against both mutant targets.

High-throughput sequencing analysis

The amplified eluates isolated from each SELEX round were subjected to next-generation sequencing (NGS), resulting in over 10^5 processed reads per round. This high-level sequence analysis enabled quantitative tracking of sequence enrichment throughout the SELEX process. Initially, read per million (RPM) values were used to rank the relative abundance of each individual sequence emerging from a round. After verifying the sequence distribution of the round 0 library (Fig. S3a–c), we first considered the top five most abundant sequences observed after the single deconvolution round for target L-TAR$_A$ (Round 5$_A$). These sequences, referred to as 5$_A$-1 through 5$_A$-5, constituted nearly half (48.5%) of the total reads found in the final pool while being considerably diverse (Fig. 2b and Fig. S5a). In addition, four out of these five sequences were further enriched in deconvolution round 5$_A$, which is in agreement with the
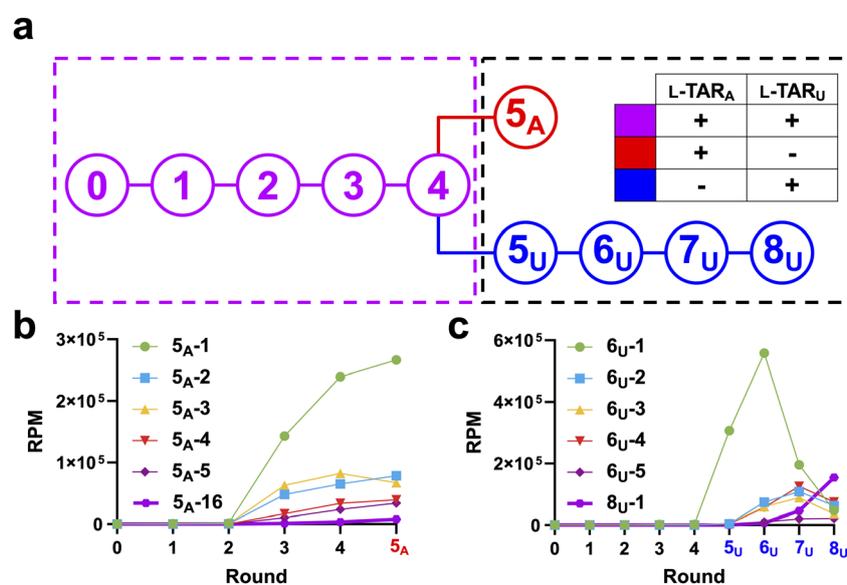
Fig. 2 Enrichment of aptamer candidates during mutagenesis–based SELEX. (a) Schematic overview of the mutagenesis–based SELEX workflow. Early selection rounds (purple) were performed against both L-TAR$_A$ and L-TAR$_U$ targets simultaneously. The black box denotes the deconvolution phase, during which the enriched pool was split and independently selected against either L-TAR$_A$ (red) or L-TAR$_U$ (blue). (b) Abundance (reads per million, RPM) of representative L-TAR$_A$-binding sequences across selection rounds. (c) Abundance (reads per million, RPM) of representative L-TAR$_U$-binding sequences across selection rounds.

© 2026 The Author(s). Published by the Royal Society of Chemistry

RSC Chem. Biol., 2026, 7, 841–850 | 843

observed prominent L-TAR$_A$ affinity of the overall pool after the initial four rounds. By tracking the abundance of these sequences through each round, we also found that the top three sequences by RPM in round 5$_A$ (5$_A$-1, 5$_A$-2, and 5$_A$-3) were already highly enriched by round 3, differing from round 5$_A$ only in their relative ranking (Fig. 2b and Fig. S6a). Not only did this result show that the population converged rapidly, but it also indicated that new cross-chiral aptamers with altered selectivity could be effectively identified within as few as three rounds of mutagenesis-based SELEX for this target.

We performed the same analysis with the L-TAR$_U$ target. The top-5 most enriched sequences in round 8$_U$, referred to as 8$_U$-1 through 8$_U$-5, demonstrated the same dominance in relative abundance, accounting for 48.8% of the total reads (Fig. S5c). Interestingly, the most abundant sequences in the final round (round 8$_U$) were also highly enriched in round 6$_U$ before plateauing or declining in later rounds (Fig. 2c and Fig. S6b, c). In fact, many of the TAR$_U$-binding sequences that became enriched early on during the deconvolution process (*e.g.*, by round 6$_U$) decreased in abundance by round 8$_U$. A plausible explanation is that sequences appearing early in the deconvolution process were simply more competitive against L-TAR$_A$-binding sequences during the mixed-pool phase of selection, even if they were not the highest-affinity L-TAR$_U$ binders. If correct, we would expect

sequences becoming more enriched during later rounds to have higher affinity towards L-TAR$_U$.

The library's unique bias towards L-TAR$_A$ in early rounds makes it an interesting case for studying specificity of cross-chiral interactions. During the deconvolution rounds for L-TAR$_U$, the absence of the L-TAR$_A$ target resulted in a drastic and rapid decrease in the abundance of the most enriched L-TAR$_A$-binding sequences (Fig. S7). This observation suggested that these sequences are highly selective for L-TAR$_A$, being able to distinguish the single nucleotide difference between the two hairpin targets. Unfortunately, the comparable analysis was not possible for L-TAR$_U$ binding sequences because the most abundant sequences in rounds 6$_U$ and 8$_U$ were not detectable by sequencing during the earlier rounds (Fig. S6b and c). However, comparison of the top enriched sequences from round 5$_A$ and 8$_U$ revealed low sequence similarities (Fig. S5a and c), adding more evidence for the specificity of emerged sequences. The selectivity of specific sequences is examined later in the study.

Comparative sequence analysis between mutant aptamers and parent L-6-4t

The mutagenized library D-Lib14 was designed to favor a low mutation rate (Fig. S3) due to our initial hypothesis that specific compensatory mutations would be able to accommodate the
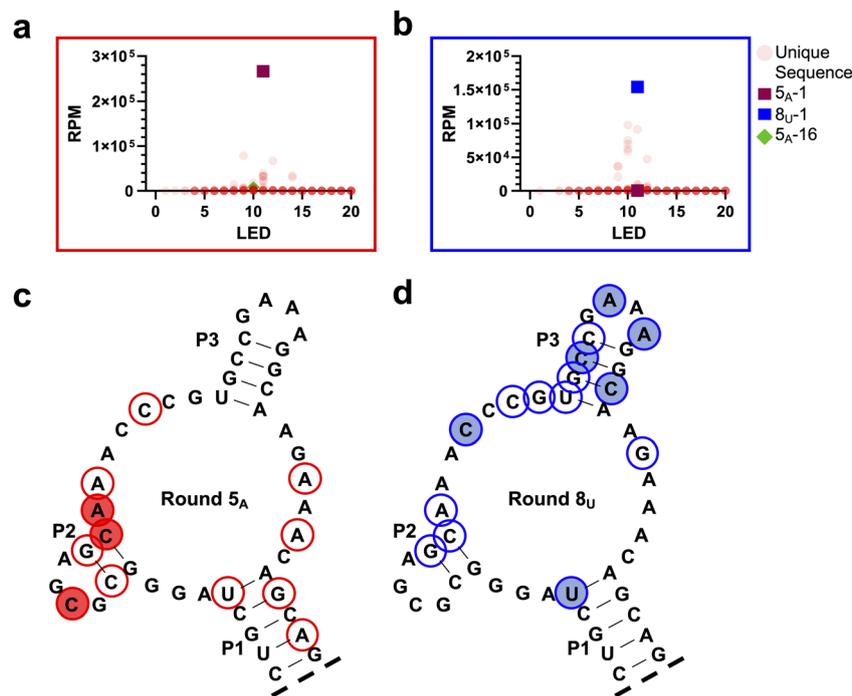
Fig. 3 Extensive sequence divergence is required to accommodate a single-nucleotide mutation in the target RNA hairpin. (a) and (b) Scatter plots showing RPM as a function of Levenshtein edit distance (LED) relative to the parent aptamer for individual sequences in round 5$_A$ (a) and 8$_U$ (b). Each semi-transparent red circle represents a unique sequence; increased color intensity reflects accumulation of distinct sequences with similar RPM and LED values. Highlighted sequences include 5$_A$-1 (magenta square), 5$_A$-16 (green diamond), and 8$_U$-1 (blue square). (c) and (d) Positions of acquired mutations in round 5$_A$ (c) and 8$_U$ (d) overlaid on the secondary structure of the parent 6-4t aptamer. The 1000 most abundant sequences from each round were used. Positions at which the evolved consensus sequences differs from the parent are circled. Filled circles indicate conversion from one base to another in the consensus, while open circles denote positions with multiple bases represented in the consensus (*i.e.*, ambiguous). Bases not circled remained unchanged in the consensus sequence compared to the parent.

844 | *RSC Chem. Biol.*, 2026, **7**, 841–850

© 2026 The Author(s). Published by the Royal Society of Chemistry

single-base mutation on the target hairpin. Therefore, we determined the Levenshtein edit distance (LED) values for each sequence compared to the parent aptamer L-6-4t. LED values measure the minimum number of single-nucleotide edits (insertions, deletions, or mutations) needed to transform one sequence into another. As deletions and insertions are only introduced through synthetic impurities and enzymatic errors, this value can be approximated to mutations in this work.

Scatter plots of individual sequences with RPM *versus* LED allows clear visualization of changes in mutation numbers among emerging sequences (Fig. 3a, b and Fig. S8). As predicted *via* our sequence distribution model, the abundance of each unique sequence is in a negative relationship to its mutation number, as seen in the starting library and enriched round 1 pool (Fig. S3a and b). However, starting at round 2, sequences with a high number of mutations (>10) started to emerge from the population, which continued through rounds 3 and 4 (Fig. S8). In the deconvolution round for L-TAR$_A$, round 5$_A$, sequences with 11 mutations were the most abundant, accounting for 49.9% of the total population (Fig. 3a and Fig. S9a). This included 5$_A$-1, the most abundant sequence overall for binding to L-TAR$_A$ (Fig. S5a). A similar trend was observed during the deconvolution rounds for L-TAR$_U$ (Fig. S8). During this process, sequences with different LED values were rapidly enriched, while remaining distributed around 11. In the terminal round for L-TAR$_U$, round 8$_U$, sequences with LED values of 10 and 11 were most abundant, attributing to 40% and 34% of the population, respectively (Fig. 3b and Fig. S9b). The most abundant sequence in round 8$_U$, 8$_U$-1, has an LED of 11 (Fig. S5c).

We next examined how mutations accumulated along the parental 6-4t aptamer sequence during selection. Although comparison of the most abundant sequences from key deconvolution rounds revealed clear differences between selections (Fig. S5), this approach captures only a limited snapshot of the evolving population. To obtain a more global view of mutational patterns, we generated consensus sequences for the round 5$_A$ and round 8$_U$ pools using the top 1000 most abundant sequences from each round, together accounting for over 90% of total sequencing reads. For each position, the consensus nucleotide was assigned as the base with the highest cumulative RPM, provided its frequency exceeded that of the second most abundant base by at least twofold; positions failing to meet this criterion were designated as ambiguous. This analysis revealed a concentration of mutation in or around the P2 stem-loop within the round 5$_A$ population (Fig. 3c). The P2 stem–loop was previously shown to be essential for binding of the parent aptamer L-6-4t to D-TAR, indicating that this region forms key contacts with the TAR hairpin. Accordingly, the single-base mutation in L-TAR$_A$ appears to have necessitated substantial reorganization of the P2 domain to preserve high-affinity binding. In contrast, far fewer mutations accumulated near P2 in the round 8$_U$ population (Fig. 3d), despite the corresponding position also being mutated in the L-TAR$_U$ target. Instead, mutations in round 8$_U$ were more concentrated around the P3 stem-loop, a region that in the parent aptamer

serves primarily as a structural element and is not thought to engage TAR directly. This shift suggests that the selection process recruited or remodeled the P3 domain to create a new functional interface capable of accommodating the transversion mutation present in L-TAR$_U$. Notably, these divergent mutational solutions highlight how selections against L-TAR$_A$ and L-TAR$_U$, which differ by only a single nucleotide, yielded aptamer families with markedly different sequence architectures.

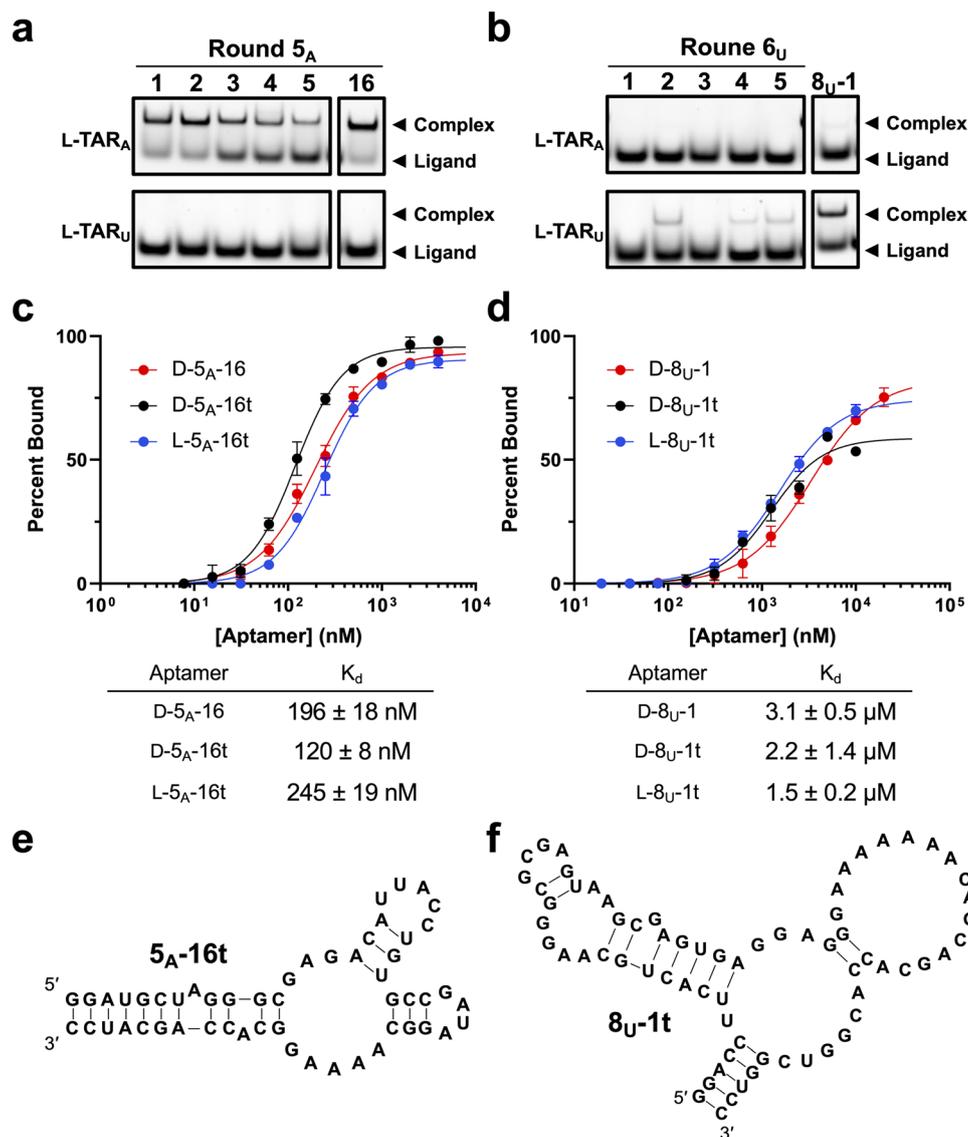## Characterization of individual aptamers

To identify lead aptamer candidates for each target, we screened the most abundant sequences emerging from the respective deconvolution rounds using EMSA (Fig. 4a and b). All sequences tested from round 5$_A$ (D-5$_A$-1 through D-5$_A$-5) bound tightly to L-TAR$_A$, with a clear correlation between sequence abundance and binding affinity. Importantly, no cross-reactivity with L-TAR$_U$ was observed (Fig. 4a), confirming the target selectivity inferred from sequencing analyses (Fig. S7).

We next evaluated sequences enriched during selection against L-TAR$_U$. Candidates from round 6$_U$ (D-6$_U$-1–D-6$_U$-5), together with a representative sequence from round 8$_U$ (D-8$_U$-1), were examined by EMSA (Fig. 4b). Sequences were intentionally chosen from multiple rounds to test the hypothesis that continued selection leads to improved binding performance. Because the most abundant sequences in round 8$_U$ were highly similar (Fig. S5c), only D-8$_U$-1 was selected for screening. Consistent with this rationale, although D-6$_U$-1 through D-6$_U$-5 displayed strong selectivity for L-TAR$_U$, their binding affinities were weaker than that of D-8$_U$-1 (Fig. 4b).

In addition to final sequence abundance, we also examined enrichment dynamics across selection rounds to identify candidates that expanded most rapidly during selection. This analysis highlighted sequence 5$_A$-16, which exhibited the largest fold enrichment between rounds 1 and 5$_A$ despite remaining at substantially lower abundance in the round 5$_A$ pool relative to other top-ranking sequences (Fig. S5a). Assuming a conservative baseline corresponding to a singleton in round 1, 5$_A$-16 increased by at least $\sim$1200-fold by round 5$_A$; because this sequence was not detected until round 3, its true enrichment is likely substantially greater. Notably, 5$_A$-16 enriched 7.7-fold between rounds 3 and 5$_A$, representing the largest enrichment over this interval among the top-ranking sequences. In contrast, the most abundant sequence, 5$_A$-1, exhibited a smaller ($\sim$380-fold) enrichment over rounds 1 to 5$_A$. Despite its lower final abundance, D-5$_A$-16 appeared to bind slightly more tightly to L-TAR$_A$ than 5$_A$-1 (Fig. 4a). While this observation is based on a single sequence and is limited by sequencing depth, it nonetheless supports prior conclusions that enrichment dynamics, rather than final abundance alone, provide a more reliable indicator of functional aptamer performance.[38,39]

Based on binding performance, subsequent analyses focused on sequences 5$_A$-16 and 8$_U$-1 (Fig. S5a and c). *In vitro* transcribed clone D-5$_A$-16 bound L-TAR$_A$ with a dissociation constant (K_d) of 196 ± 18 nM, whereas clone D-8$_U$-1 bound

© 2026 The Author(s). Published by the Royal Society of Chemistry

RSC Chem. Biol., 2026, **7**, 841–850 | **845**

Fig. 4 Functional characterization of evolved aptamer candidates. (a) and (b) EMSA analysis (10% native PAGE; 19:1 acrylamide:bis-acrylamide) of representative D-aptamers binding to L-TAR$_A$ (a) or L-TAR$_U$ (b). Reactions contained 1 μM aptamer and 5 nM FAM-labeled target RNA in 25 mM Tris (pH 7.6), 50 mM NaCl, 10 mM MgCl$_2$, and 8% (v/v) glycerol, and were incubated at 23 °C for 30 min prior to separation. (c) and (d) Binding isotherms derived from EMSA experiments used to determine apparent dissociation constants (K_d) for full-length and truncated aptamers binding their cognate targets. Data represent mean ± S.D. from three independent experiments (n = 3). Standard EMSA conditions were used, except that aptamer concentrations were varied while maintaining the corresponding cognate cross-chiral aptamer–target pair. (e) and (f) Predicted secondary structures of truncated aptamer clones L-5$_A$-16t (e) and L-8$_U$-1t (f).

L-TAR$_U$ with substantially weaker affinity (K_d = 3.1 ± 0.5 μM; Fig. 4c and d). Although both aptamers exhibited reduced affinity relative to the parental L-6-4t aptamer binding to D-TAR (K_d = 100 ± 30 nM),[23] the loss in binding strength was far more pronounced for D-8$_U$-1, which displayed a >30-fold increase in K_d. This pronounced difference likely reflects the distinct structural consequences of the target mutations. The transversion mutation present in L-TAR$_U$ is expected to introduce a larger perturbation to the RNA hairpin geometry than the corresponding transition mutation in L-TAR$_A$, posing a greater challenge for shape-based, cross-chiral recognition. Consistent with this interpretation, sequences binding L-TAR$_A$ dominated the early rounds of selection, suggesting that smaller structural deviations from the parental TAR hairpin are more readily accommodated. Notably, analysis of predicted secondary structures revealed that neither evolved aptamer retains appreciable similarity to the parental L-6-4t structure (Fig. S10a and e). Together, these findings suggest that even single-nucleotide changes in the target RNA can necessitate extensive remodeling of the aptamer fold, highlighting the complexity of cross-chiral, structure-based recognition and the need for coordinated, multi-site mutational networks to restore high-affinity binding.
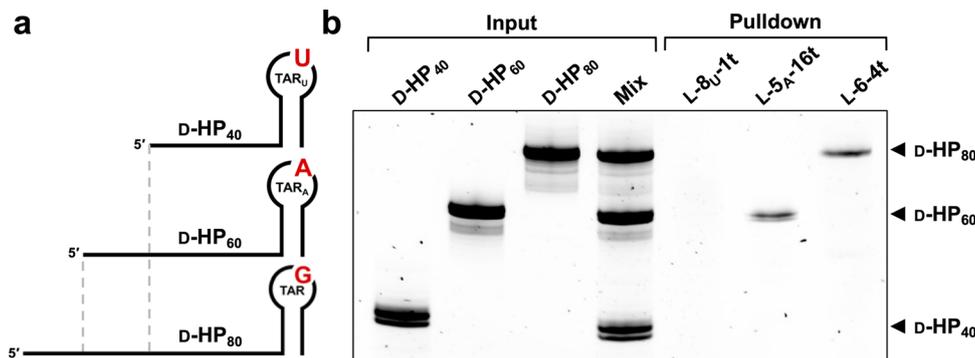
Fig. 5 Specific recovery of RNA transcripts with embedded hairpin structures. (a) Illustration of three RNA transcripts with different lengths bearing a hairpin structure at 3′ terminal. (b) Denaturing PAGE analysis of the L-aptamer–based affinity pulldown experiment.

Preparation of truncated L-RNA aptamers

We sought to remove non-essential nucleotides from 5_A-16 and 8_U-1, being 79-nt and 78-nt in length, to improve downstream synthesis and potentially increase affinity due to reduced steric effect.[22–24] Rational truncation of both aptamers was performed based on predicted secondary structures (Fig. S10a–h). Both sequences tolerated only mild truncations of potentially non-functional duplex-forming sequence at both ends. The resulting truncations yielded sequences 5_A-16t and 8_U-1t (Fig. 4e and f). D-5_A-16t and D-8_U-1t bound to their corresponding L-RNA targets with K_d values of 120 ± 5 nM and 2.2 ± 1.4 µM, respectively (Fig. 4c and d). The affinity of both aptamers improved after truncation, similar to what has been observed with prior cross-chiral aptamers.[22–24,26] Interestingly, aptamer D-8_U-1t displayed self-inhibitory activity at higher concentration, which was not observed for the full-length sequence (Fig. 4d). We speculated that the truncation removed structural constraints present in the full-length aptamer, promoting formation of nonproductive structures (e.g., dimers) at higher concentrations.

Both truncated aptamers were then prepared in the L-RNA form through solid-phase chemical synthesis using L-ribonucleoside phosphoramidites (Fig. S11). L-5_A-16t bound to D-TAR_A with a K_d of 245 ± 19 nM, while L-8_U-1t bound to D-TAR_U with a K_d of 1.5 ± 0.2 µM. Due to the reduced quality of synthetic L-RNA compared to enzymatically prepared D-RNA, it is not uncommon for L-aptamers to have slight increase in K_d values relative to their D-RNA counterparts.[22–24,26] The apparent *increase* in affinity observed for L-8_U-1t is likely an artifact of the self-inhibitory behavior that complicates accurate binding quantification. Notably, cross-reactivity was evaluated by EMSA across all aptamer–ligand combinations. No binding was observed to non-cognate targets, and L-aptamers bound exclusively to the corresponding D-RNA targets, with no detectable interaction with the L-RNA counterparts (Fig. S12).

Orthogonal recognition of structured RNA targets by cross-chiral aptamers

A central goal of this study was to generate aptamers that exhibit high specificity and orthogonality toward closely related structured RNA targets. To evaluate aptamer performance beyond EMSA, we employed an RNA pulldown experiment to directly assess target discrimination in a competitive and more structurally complex context. A mixture of three RNA transcripts, D-HP_{80}, D-HP_{60}, and D-HP_{40}, was prepared, each containing a terminal hairpin structure with distal loop sequences corresponding to TAR, TAR_A, and TAR_U, respectively (Fig. 5a). These transcripts differed in overall length, allowing them to be readily distinguished by denaturing PAGE. 5′-Biotinylated L-aptamers (L-5_A-16t, L-8_U-1t, and L-6-4t) were individually immobilized on streptavidin-coated magnetic beads and incubated with the RNA mixture. Following washing, the captured RNA was analyzed by denaturing PAGE, with transcript identity resolved by length (Fig. 5b). The pulldown results were fully consistent with EMSA-based binding measurements. Both L-5_A-16t and L-6-4t selectively recovered RNA transcripts containing their cognate target sequences, with no detectable capture of non-cognate RNAs. Under the stringency of this competitive assay, L-8_U-1t did not recover measurable RNA, consistent with its weaker affinity for D-TAR_U determined by EMSA, and did not exhibit any nonspecific interactions. Importantly, this assay was performed in the presence of extended flanking sequences and direct competition among multiple structured RNA targets. The retention of strict target selectivity under these conditions highlights the robustness of the evolved aptamers and underscores their potential as highly specific and orthogonal RNA-binding reagents.

Conclusion

In this study, we demonstrate that mutagenesis-based SELEX can be successfully applied to cross-chiral aptamers to rapidly reprogram target specificity while maintaining high selectivity. Starting from a single parental L-aptamer, this approach yielded two evolved aptamers, L-5_A-16t and L-8_U-1t, which together with the original L-6-4t form a set of three orthogonal RNA-binding reagents capable of discriminating RNA hairpins that differ by only a single nucleotide. By combining deep sequencing with enrichment analysis, we show that this process is rapid and highly informative. Cross-chiral aptamers with altered target selectivity can be identified within three or fewer selection

© 2026 The Author(s). Published by the Royal Society of Chemistry

RSC Chem. Biol., 2026, **7**, 841–850 | **847**

rounds, underscoring the speed and efficiency of this approach. At the same time, the sequencing data reveal that retargeting efficiency is sensitive to the degree of structural perturbation in the target RNA, as illustrated by the distinct evolutionary trajectories observed for the TAR_U variant. Importantly, analysis of sequence evolution and predicted secondary structures revealed that accommodation of even a single-nucleotide change in the target does not arise from local or incremental adjustments to the parental aptamer. Instead, both transition and transversion mutations in the target RNA necessitated extensive restructuring of the aptamer fold through complex, distributed mutation networks. These observations underscore a defining advantage of cross-chiral aptamers: their ability to recognize RNA targets through global structure and tertiary architecture rather than sequence complementarity. As a result, cross-chiral aptamers can achieve levels of specificity and single-nucleotide discrimination that are difficult to realize with hybridization-based approaches such as antisense oligonucleotides, which rely primarily on Watson–Crick base pairing and are often insensitive to subtle but functionally important structural differences.[40,41] Structure-based recognition enables selective targeting of conformationally distinct RNA states, providing a powerful means to discriminate between closely related RNAs that differ minimally in sequence but meaningfully in shape.

While the present conclusions are derived from a defined set of cross-chiral aptamer–hairpin pairs, the broader implications extend well beyond the TAR system. RNA hairpins and stem–loop motifs are ubiquitous in biology, serving as regulatory elements, protein-binding platforms, and conserved functional structures in viral and cellular RNAs.[1,42] Unlike hybridization-based approaches such as antisense oligonucleotides or siRNAs, which rely on Watson–Crick base pairing and therefore require access to linear sequence elements, cross-chiral aptamers recognize RNA targets through tertiary structure and global shape complementarity.[16] This feature may enable selective targeting of structured RNA motifs that are difficult to access using traditional hybridization-based technologies. The ability to rapidly retarget an existing aptamer to closely related structural variants offers a practical route to generate new reagents against evolving RNA targets, such as viral genomes that accumulate point mutations during strain evolution while preserving overall secondary structure. In this context, mutagenesis-based evolution enables parallel diversification of aptamer specificity from a common scaffold, allowing rapid adaptation to emerging variants without restarting the selection process. Future applications of this framework could extend beyond the single-nucleotide loop mutations examined here to explore larger sequence and structural perturbations, further defining the scope and adaptability of cross-chiral aptamer evolution. While mutagenesis-based selection is inherently biased toward sequence space proximal to the parental aptamer, the substantial mutational divergence and structural remodeling observed here indicate that this approach can access a diverse range of sequence and structural solutions. Nonetheless, *de novo* selection from fully randomized libraries

may yield alternative aptamer architectures with distinct and potentially improved binding properties, and these strategies should therefore be viewed as complementary depending on the intended application. Importantly, even within the limited sequence space examined here, the robustness of the evolved aptamers is already evident. RNA pulldown experiments demonstrated that the evolved aptamers retain strict target selectivity in a competitive and structurally complex environment that includes extended flanking sequences and multiple RNA species. The maintenance of orthogonality under these conditions underscores their robustness and highlights their potential for diverse applications, including RNA-selective biosensors, diagnostic tools, and affinity reagents for isolating specific structured RNAs from complex biological samples.[30] An important future direction will be structural characterization of cross-chiral aptamer–RNA complexes to better understand the molecular basis of these interactions. While current computational prediction tools are largely optimized for natural biopolymers, advances in RNA structural biology and modeling may eventually enable high-resolution characterization of cross-chiral recognition mechanisms.

Recent discussions surrounding mirror-life have emphasized the possibility that mirror biopolymers could be largely orthogonal to natural biological systems.[43] However, cross-chiral aptamers provide clear experimental examples of selective molecular recognition between mirror-image nucleic acids. The results presented here further demonstrate that such cross-chiral interactions can evolve to discriminate structured RNA targets that differ by only a single nucleotide, highlighting the precision achievable through tertiary, structure-based recognition. These findings illustrate that while mirror biopolymers are incompatible with canonical Watson–Crick hybridization, highly specific interactions between chiral systems can nevertheless arise through alternative structural recognition mechanisms.

Taken together, this work establishes mutagenesis-based SELEX as a versatile strategy for rapidly reprogramming cross-chiral L-aptamers and reinforces the unique advantages of structure-based RNA recognition for discriminating closely related structured RNA targets. More broadly, it provides a framework for developing adaptable RNA-targeting reagents capable of keeping pace with dynamic and mutating RNA landscapes, positioning cross-chiral aptamers as powerful tools in chemical biology and RNA-focused biotechnology.

Author contributions

Xuan Han: methodology, investigation, formal analysis, visualization, writing – original draft. Tyler Guilbault: methodology, investigation, formal analysis, visualization. Jonathan T. Sczepanski: conceptualization, formal analysis, writing – original draft, supervision, project administration, funding acquisition.

Conflicts of interest

There are no conflicts to declare.

848 | *RSC Chem. Biol.,* 2026, **7**, 841–850

© 2026 The Author(s). Published by the Royal Society of Chemistry

Data availability

The data supporting this article have been included as part of the supplementary information (SI). Supplementary information: Fig. S1–S19 and Tables S1, S2, reagents and experimental methods, oligonucleotides sequences and structures, mass spectra of oligonucleotides, gel electrophoresis images, and DNA sequencing data. See DOI: https://doi.org/10.1039/d6cb00057f.

Acknowledgements

References

1 X. Cao, Y. Zhang, Y. Ding and Y. Wan, Identification of RNA structures and their roles in RNA functions, *Nat. Rev. Mol. Cell Biol.*, 2024, **25**(10), 784–801.

2 Y. Zhang, J. Qian, C. Gu and Y. Yang, Alternative splicing and cancer: a systematic review, *Signal Transduction Targeted Ther.*, 2021, **6**(1), 78.

3 Q. Peng, Y. Zhou, L. Oyang, N. Wu, Y. Tang, M. Su, X. Luo, Y. Wang, X. Sheng, J. Ma and Q. Liao, Impacts and mechanisms of alternative mRNA splicing in cancer metabolism, immune response, and therapeutics, *Mol. Ther.*, 2022, **30**(3), 1018–1035.

4 Y. Peng and C. M. Croce, The role of MicroRNAs in human cancer, *Signal Transduction Targeted Ther.*, 2016, **1**(1), 15004.

5 B. Malone, N. Urakova, E. J. Snijder and E. A. Campbell, Structures and functions of coronavirus replication–transcription complexes and their relevance for SARS-CoV-2 drug design, *Nat. Rev. Mol. Cell Biol.*, 2022, **23**(1), 21–39.

6 T. Osawa, M. Aoki, H. Ehara and S.-I. Sekine, Structures of dengue virus RNA replicase complexes, *Mol. Cell*, 2023, **83**(15), 2781–2791.e4.

7 R. G. Huber, X. N. Lim, W. C. Ng, A. Y. L. Sim, H. X. Poh, Y. Shen, S. Y. Lim, K. B. Sundstrom, X. Sun, J. G. Aw, H. K. Too, P. H. Boey, A. Wilm, T. Chawla, M. M. Choy, L. Jiang, P. F. de Sessions, X. J. Loh, S. Alonso, M. Hibberd, N. Nagarajan, E. E. Ooi, P. J. Bond, O. M. Sessions and Y. Wan, Structure mapping of dengue and Zika viruses reveals functional long-range interactions, *Nat. Commun.*, 2019, **10**(1), 1408.

8 P. K. Todd and H. L. Paulson, RNA-mediated neurodegeneration in repeat expansion disorders, *Ann. Neurol.*, 2010, **67**(3), 291–300.

9 A. Baud, M. Derbis, K. Tutak and K. Sobczak, Partners in crime: proteins implicated in RNA repeat expansion diseases, *WIREs RNA*, 2022, **13**(4), e1709.

10 Y. Sun, H. Dai, X. Dai, J. Yin, Y. Cui, X. Liu, G. Gonzalez, J. Yuan, F. Tang, N. Wang, A. E. Perlegos, N. M. Bonini, X. W. Yang, W. Gu and Y. Wang, m1A in CAG repeat RNA binds to TDP-43 and induces neurodegeneration, *Nature*, 2023, **623**(7987), 580–587.

11 A. Chini, P. Guha, V. S. Malladi, Z. Guo and S. S. Mandal, Novel long non-coding RNAs associated with inflammation and macrophage activation in human, *Sci. Rep.*, 2023, **13**(1), 4036.

12 S. R. Nallagatla, R. Toroney and P. C. Bevilacqua, Regulation of innate immunity through RNA structure and the protein kinase PKR, *Curr. Opin. Struct. Biol.*, 2011, **21**(1), 119–127.

13 S. Ando, S. Suzuki, S. Okubo, K. Ohuchi, K. Takahashi, S. Nakamura, M. Shimazawa, K. Fuji and H. Hara, Discovery of a CNS penetrant small molecule SMN2 splicing modulator with improved tolerability for spinal muscular atrophy, *Sci. Rep.*, 2020, **10**(1), 17472.

14 R. Aguilar, K. B. Spencer, B. Kesner, N. F. Rizvi, M. D. Badmalia, T. Mrozowich, J. D. Mortison, C. Rivera, G. F. Smith, J. Burchard, P. J. Dandliker, T. R. Patel, E. B. Nickbarg and J. T. Lee, Targeting Xist with compounds that disrupt RNA structure and X inactivation, *Nature*, 2022, **604**(7904), 160–166.

15 J. L. Childs-Disney, X. Yang, Q. M. R. Gibaut, Y. Tong, R. T. Batey and M. D. Disney, Targeting RNA structures with small molecules, *Nat. Rev. Drug Discovery*, 2022, **21**(10), 736–762.

16 B. S. E. Heale, H. S. Soifer, C. Bowers and J. J. Rossi, siRNA target site secondary structure predictions using local stable substructures, *Nucleic Acids Res.*, 2005, **33**(3), e30–e30.

17 H. Ratni, R. S. Scalco and A. H. Stephan, Risdiplam, the First Approved Small Molecule Splicing Modifier Drug as a Blueprint for Future Transformative Medicines, *ACS Med. Chem. Lett.*, 2021, **12**(6), 874–877.

18 C. Tuerk and L. Gold, Systematic evolution of ligands by exponential enrichment: RNA ligands to bacteriophage T4 DNA polymerase, *Science*, 1990, **249**(4968), 505–510.

19 H. Qu, A. T. Csordas, J. Wang, S. S. Oh, M. S. Eisenstein and H. T. Soh, Rapid and Label-Free Strategy to Isolate Aptamers for Metal Ions, *ACS Nano*, 2016, **10**(8), 7558–7565.

20 M. Guérin, M. Vandevenne, A. Matagne, W. Aucher, J. Verdon, E. Paoli, J. Ducrotoy, S. Octave, B. Avalle, I. Maffucci and S. Padiolleau-Lefèvre, Selection and characterization of DNA aptamers targeting the surface Borrelia protein CspZ with high-throughput cross-over SELEX, *Commun. Biol.*, 2025, **8**(1), 632.

21 K. Sefah, D. Shangguan, X. Xiong, M. B. O'Donoghue and W. Tan, Development of DNA aptamers using Cell-SELEX, *Nat. Protoc.*, 2010, **5**(6), 1169–1185.

22 J. T. Sczepanski and G. F. Joyce, Specific Inhibition of MicroRNA Processing Using L-RNA Aptamers, *J. Am. Chem. Soc.*, 2015, **137**(51), 16032–16037.

23 J. T. Sczepanski and G. F. Joyce, Binding of a Structured D-RNA Molecule by an L-RNA Aptamer, *J. Am. Chem. Soc.*, 2013, **135**(36), 13290–13293.

24 J. Li and J. T. Sczepanski, Targeting a conserved structural element from the SARS-CoV-2 genome using L-DNA aptamers, *RSC Chem. Biol.*, 2022, **3**(1), 79–84.

© 2026 The Author(s). Published by the Royal Society of Chemistry

RSC Chem. Biol., 2026, **7**, 841–850 | 849

25 A. M. Kabza and J. T. Sczepanski, An L-RNA Aptamer with Expanded Chemical Functionality that Inhibits MicroRNA Biogenesis, *ChemBioChem*, 2017, **18**(18), 1824–1827.

26 S. Dey and J. T. Sczepanski, In vitro selection of L-DNA aptamers that bind a structured D-RNA molecule, *Nucleic Acids Res.*, 2020, **48**(4), 1669–1680.

27 M. I. Umar, C.-Y. Chan and C. K. Kwok, Development of RNA G-quadruplex (rG4)-targeting L-RNA aptamers by rG4-SELEX, *Nat. Protoc.*, 2022, **17**(6), 1385–1414.

28 S. Y. Lam, M. I. Umar, H. Zhao, J. Zhao and C. K. Kwok, Capture of RNA G-quadruplex structures using an L-RNA aptamer, *RSC Chem. Biol.*, 2024, **5**(10), 1045–1051.

29 D. Ji, J.-H. Yuan, S.-B. Chen, J.-H. Tan and C. K. Kwok, Selective targeting of parallel G-quadruplex structure using L-RNA aptamer, *Nucleic Acids Res.*, 2023, **51**(21), 11439–11452.

30 V. Shearer, C.-H. Yu, X. Han and J. T. Sczepanski, The clinical potential of L-oligonucleotides: challenges and opportunities, *Chem. Sci.*, 2024, **15**(44), 18239–18258.

31 A. T. Piwko, X. Han, A. M. Kabza, S. Dey and J. T. Sczepanski, Inverse In Vitro Selection Enables Comprehensive Analysis of Cross-Chiral L-Aptamer Interactions, *ChemBioChem*, 2022, **23**(24), e202200520.

32 C. Olea, J. Weidmann, P. E. Dawson and G. F. Joyce, An L-RNA Aptamer that Binds and Inhibits RNase, *Chem. Biol.*, 2015, **22**(11), 1437–1441.

33 Z. Huang and J. W. Szostak, Evolution of aptamers with a new specificity and new secondary structures from an ATP aptamer, *RNA*, 2003, **9**(12), 1456–1463.

34 F. Wachowius, B. T. Porebski, C. M. Johnson and P. Holliger, Emergence of ATP- and GTP-Binding Aptamers from Single RNA Sequences by Error-Prone Replication and Selection, *ChemSystemsChem*, 2023, **5**(5), e202300006.

35 S. Klußmann, A. Nolte, R. Bald, V. A. Erdmann and J. P. Fürste, Mirror-image RNA that binds D-adenosine, *Nat. Biotechnol.*, 1996, **14**(9), 1112–1115.

36 K. P. Williams, X.-H. Liu, T. N. M. Schumacher, H. Y. Lin, D. A. Ausiello, P. S. Kim and D. P. Bartel, Bioactive and nuclease-resistant L-DNA ligand of vasopressin, *Proc. Natl. Acad. Sci. U. S. A.*, 1997, **94**(21), 11285–11290.

37 A. Nolte, S. Klußmann, R. Bald, V. A. Erdmann and J. P. Fürste, Mirror-design of L-oligonucleotide ligands binding to L-arginine, *Nat. Biotechnol.*, 1996, **14**(9), 1116–1119.

38 T. Singh, R. Fogel and J. Limson, NGS-Guided Aptamer Re-Selection for Improved Sensor Applications: Biotin as a Modification Tag in the Amplification of Enriched Pools, *Eng. Proc.*, 2025, **109**(1), 7.

39 R. Didarian, H. K. Ozbek, V. C. Ozalp, O. Erel and N. Yildirim-Tirgil, Enhanced SELEX Platforms for Aptamer Selection with Improved Characteristics: A Review, *Mol. Biotechnol.*, 2025, **67**(8), 2962–2977.

40 J. Scharner, W. K. Ma, Q. Zhang, K.-T. Lin, F. Rigo, C. F. Bennett and A. R. Krainer, Hybridization-mediated off-target effects of splice-switching antisense oligonucleotides, *Nucleic Acids Res.*, 2020, **48**(2), 802–816.

41 P. Andersson, S. A. Burel, H. Estrella, J. Foy, P. H. Hagedorn, T. A. Harper, S. P. Henry, J.-C. Hoflack, E. M. Holgersen, A. A. Levin, E. Morrison, A. Pavlicek, L. Penso-Dolfin and U. Saxena, Assessing Hybridization-Dependent Off-Target Risk for Therapeutic Oligonucleotides: Updated Industry Recommendations, *Nucleic Acid Ther.*, 2025, **35**(1), 16–33.

42 P. Svoboda and A. D. Cara, Hairpin RNA: a secondary structure of primary importance, *Cell. Mol. Life Sci.*, 2006, **63**(7), 901–908.

43 K. P. Adamala, D. Agashe, Y. Belkaid, D. M. D. C. Bittencourt, Y. Cai, M. W. Chang, I. A. Chen, G. M. Church, V. S. Cooper, M. M. Davis, N. K. Devaraj, D. Endy, K. M. Esvelt, J. I. Glass, T. W. Hand, T. V. Inglesby, F. J. Isaacs, W. G. James, J. D. G. Jones, M. S. Kay, R. E. Lenski, C. Liu, R. Medzhitov, M. L. Nicotra, S. B. Oehm, J. Pannu, D. A. Relman, P. Schwille, J. A. Smith, H. Suga, J. W. Szostak, N. J. Talbot, J. M. Tiedje, J. C. Venter, G. Winter, W. Zhang, X. Zhu and M. T. Zuber, Confronting risks of mirror life, *Science*, 2024, **386**(6728), 1351–1353.